Investigation of Heat Transfer Characteristics of an Internally Heated Fluid in Horizontal Laminar Pipe Flow

Dong-Hyuk Park and Bum-Jin Chung*
Department of Nuclear Engineering, Kyung Hee University
#1732 Deogyeong-daero, Giheung-gu, Yongin-si, Gyeonggi-do, 17104, Korea
*Corresponding author: bjchung@khu.ac.kr

*Keywords: Internal heat generation; Molten salt reactor; Laminar flow; Secondary flow

1. Introduction

In the liquid fueled Molten Salt Reactors (MSRs), the nuclear fuel is dissolved in the coolant [1–2]. Therefore, the heat source resides within the fluid volume itself rather than external boundary, compared to the conventional solid fuel nuclear reactor. The Internal Heat Generation (IHG) in MSRs is not confined in the reactor core since the decay heat persist in the out of core component, such as pipeline, heat exchanger, and reprocessing system. This unique thermal condition requires a detailed understanding of how IHG influences temperature distributions and heat transfer characteristics in MSRs.

Despite its significance, research on the IHG in forced convection remains limited [3–6]. Most conventional heat transfer studies focus on wall heating or cooling, as these are the dominant modes in traditional systems. In contrast, volumetric heat sources within the fluid are uncommon, aside from special cases such as exothermic chemical reactions or nuclear reactors such as MSRs. As a result, the thermal-hydraulic behavior induced by the IHG has not been thoroughly investigated [7]. The detailed literature reviews for IHG can be found in our previous study [8].

In this study, we experimentally investigate the thermal-hydraulic characteristics of the laminar pipe flow with internal heat generation under adiabatic wall conditions. To simulate IHG, an alternating current was applied to an electrically conducting fluid. Axial and circumferential wall temperature profiles were measured varying the Reynolds number (Re) and the volumetric heat generation rate (q). Based on the measured data, a correlation for the non-dimensional temperature difference was developed to quantify the thermal behavior under IHG conditions.

2. Experimental setup

2.1) Experimental apparatus

In this study, the IHG was simulated by electrical dissipation of an electrolyte fluid by applying alternating current to an electrolyte solution. Fig. 1 shows the schematic diagram of the experimental loop. The working fluid, consisting of a 0.1–2 wt% sulfuric acid solution, was continuously circulated through the loop using a centrifugal chemical pump (PM-250PMS,

WILO). The fluid sequentially passed through a flowmeter (DMA20, Picomag), a hydrodynamic entrance section, the test section, a downstream mixing section, and finally returned to the reservoir.

Due to the corrosivity of sulfuric acid solution, the test section was composed of chlorinated polyvinyl chloride (C-PVC) pipes, each with an inner diameter of 30 mm and a length of 0.5 m. C-PVC was selected due to its superior thermal resistance (up to 95 °C). Three graphite ring electrodes (inner diameter: 30 mm, length: 50 mm) were embedded within flanges located at the front, center, and rear of the test section. These electrodes served as electrical contact points and physical connectors between test section segments. A total of 24 K-type thermocouples were installed at eight equally spaced axial locations along the pipe.

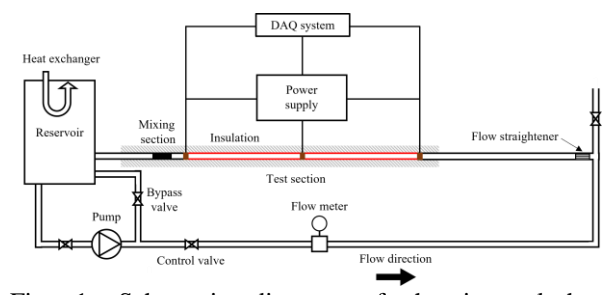


Fig. 1. Schematic diagram of the internal heat generation experimental loop.

To generate uniform volumetric heat generation, a high-frequency alternating current (260 Hz) was passed through the working fluid in the test section. The use of high frequency was intended to suppress electrolysis, which commonly occurs at lower frequencies in electrolytic solutions. A single-phase 220 V AC (60 Hz) source was connected to a variable autotransformer (SV-5023, DAEWKWNG T&M) to adjust the input voltage, which was then converted to a 260 Hz three-phase AC signal via an inverter (LSLV0022M100, LS Electric).

To measure the wall temperature distribution, twenty-four K-type thermocouples were installed at eight equally spaced axial locations along the pipe. At each axial location, three thermocouples were arranged circumferentially (top, side, and bottom) to capture local variations. Unlike metal pipes, CPVC has low thermal conductivity; thus, thermocouples were not welded to the surface but inserted through precisely

drilled holes, directly contacting the fluid inside. To prevent leakage, each thermocouple wire was passed through a silicone tube and sealed with a silicone-based adhesive. The entire test section was wrapped in fiberglass insulation to minimize external heat loss.

All experimental data were recorded using a National Instruments (NI) data acquisition system. Temperature measurements were collected through NI-9212 modules, which provide channel-to-channel isolation up to 250 Vrms, minimizing electrical interference from the current passing through the test section. The electrical current and voltage were measured using the NI-9247 and NI-9225 modules, respectively, ensuring accurate and synchronized data logging

2.2) Data processing

Since the alternative current flows through the test section, the average power of internal heat generation (Q) was calculated using the measured values of current and voltage as follows:

$$Q = \frac{1}{t_2 - t_1} \int_{t_1}^{t_2} V(t)I(t)dt \,. \tag{1}$$

The corresponding volumetric heat generation rate (q) was then calculated as follows:

$$q = Q / (\pi r_0^2 L) \tag{2}$$

where L and r_o is the length and radius of the test section, respectively. According to the energy conservation law, the local bulk fluid temperature at location x, $T_b(x)$, was estimated as follows:

$$q\pi r_0^2 x = \pi r_0^2 \rho c_n u_m (T_b(x) - Ti)$$
 (3)

$$T_{b}(x) = (qx / \rho c_{p} u_{m}) + T_{s}.$$
 (4)

The average wall temperature at each axial location was calculated by averaging the three circumferentially measured wall temperatures.

$$T_{w} = \frac{T_{w,-90^{\circ}} + 2T_{w,0^{\circ}} + T_{w,90^{\circ}}}{A}.$$
 (5)

For the IHG flow, the non-dimensional wall to bulk fluid temperature difference, which is denoted as Θ in this study, is expressed as follows:

$$\Theta = \frac{k(T_{w} - T_{b})}{qr^{2}} \,. \tag{6}$$

This parameter is analogous to the inverse of the Nusselt number in wall heating heat transfer. This relation becomes evident when the denominator is rewritten as qr_0/k , where qr_0 has the dimensions of heat flux. To represent the natural convection effect in IHG flow, the modified Grashof number (Gr^*) was calculated as follows:

$$Gr^* = \frac{g\beta qD^5}{v^2k} \,. \tag{7}$$

The non-dimensional axial distance (X^+) was calculated as Eq. (8). This parameter is widely used in forced convection laminar heat transfer and represents the growth of the thermal boundary layer along the flow direction. Sparrow [5] demonstrated that, even in flows with IHG the dimensionless temperature variation (Θ) can be normalized by X^+

$$X^{+} = (x/D)/RePr. (8)$$

2.3) Test matrix

Table 1 presents the test matrix for the present work. The inner diameter (D) of test section was set at 0.03 m and its length (L) was 1.15 m. Pr ranged from 5.75 to 6.1. The Re ranged from 630 to 1290 and q was adjusted between 1.09 $\times 10^5$ and 1.09 $\times 10^6$ W/m³ by altering the concentration of sulfuric acid and applied voltage. The corresponding Gr^* ranged from 1.84 $\times 10^7$ to 2.15 $\times 10^8$.

Table 1. Test matrix.

Pr	Re	$q (W/m^3)$	Gr^*
5.75-6.10	630–1290	1.09×10^{5}	$1.84 \times 10^{7} -$
		$^{-1.09\times10^{6}}$	2.15×10^{8}

3. Results and discussion

3.1) Data validation

Figure 2 compares the axial profiles of $\Theta_{avg}(\Omega)$ m the present results with Sparrow and Siegel's result [5]. The closed symbols represent the experimental results for the lowest q cases with different Re. The solid black line indicates the Theoretical Pure Forced Convection (TPFC) result from Sparrow and Siegel [5] in which buoyancy effect is not incorporated. The black circular symbols representing the case with the lowest Re showed good agreement with the results from the existing studies. The relative error remained within 10% compared to the TPFC results.

However, as Re increased, the Θ_{avg} deviates from the TPFC result and became lower. This discrepancy is attributed to the natural convection effect, which will be discussed in detail in Section 3.3.

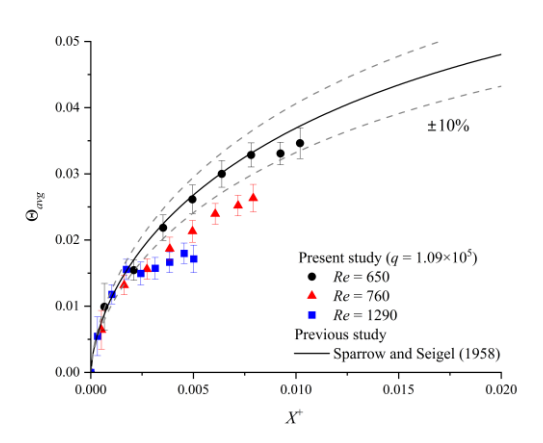


Fig. 2. Comparison of the axial profiles of Θ_{avg} from the present experimental results with previous studies conducted by Sparrow and Siegel [5].

3.2) Temperature distribution in pure forced convection IHG flow

When the IHG occurs within the flow, the resulting temperature distribution is strongly influenced by the local fluid velocity. Near the wall, the fluid velocity decreases due to the wall friction, which increases the heating time by the IHG. As a result, the temperature rise is more pronounced at the near-wall region. Fig. 3 shows the axial wall and bulk fluid temperature distribution in pure forced convection IHG flow case (Re = 630, $q = 1.09 \times 10^5$ W/m3). The wall temperature was higher than the bulk fluid temperature due to wall friction. Such pure forced convection behavior was observed only when the wall temperature increase was relatively low.

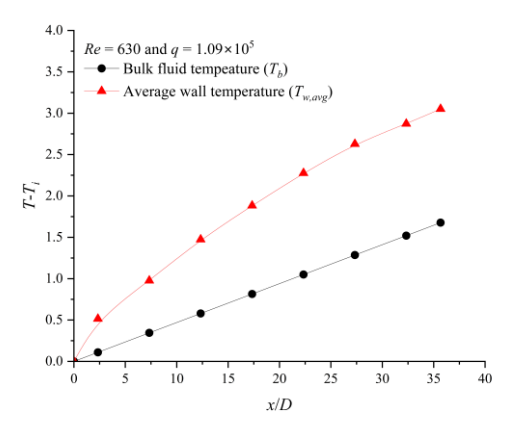


Fig. 3. Comparison of axial wall and bulk fluid temperature distributions in the pure forced convection (Re = 630, $q = 1.09 \times 10^5 \text{ W/m}^3$).

3.3) Influence of buoyancy force on temperature distribution in IHG flow

As the wall temperature increased sufficiently, the deviation from the TPFC result was observed. This deviation is attributed to the buoyancy force induced by

the IHG. Fig. 4 shows the circumferential wall temperature distribution along the axial locations for Re = 760 and $q = 2.71 \times 105$ W/m³. An increase in wall temperature was observed from the bottom point ($\theta = -$ 90°) to the top point ($\theta = 90$ °). Due to the higher fluid temperature near the wall, owing to the longer exposure of the IHG, a radial temperature gradient is formed between the wall and the pipe center, which induces buoyancy forces. These forces cause the hotter fluid near the wall to rise and accumulate at the upper region of the pipe. As the flow develops downstream, this thermal stratification becomes more pronounced, in larger circumferential resulting temperature variations along the axial direction.

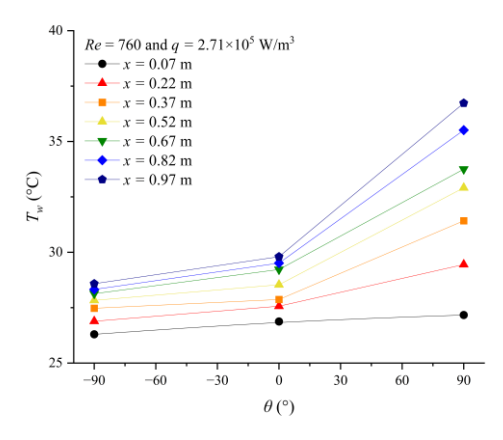


Fig. 4. Influence of buoyancy force on circumferential wall temperature distribution with different axial location (Re = 735, $q = 2.71 \times 10^5$ W/m3).

As illustrated in Fig. 5, a D-shaped secondary flow is induced, characterized by upward motion near the wall and downward motion at the pipe center. This D-shaped secondary flow promotes enhanced flow mixing beneath the thermally stagnant region, thereby reducing the wall temperature compared to that observed under pure forced convection conditions.

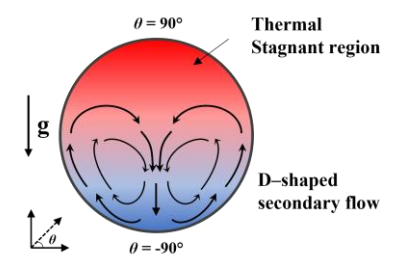


Fig. 5. An illustration of buoyancy-driven D-shaped secondary flow in IHG flow.

Figure 6 shows the influence of buoyancy force on Θ along the X^+ . The dashed line represents the TPFC results reported by Sparrow and Siegel [5]. Since Θ denotes the non-dimensional temperature difference between the wall and the bulk fluid, it tends to increase under thermally stagnant conditions and decrease when

flow mixing is enhanced. As shown in Fig. 9, the Θ at θ =90° is higher than the TPFC due to thermal stagnation, while Θ at θ = -90° and 0° is lower than TPFC due to the D-shaped secondary flow.

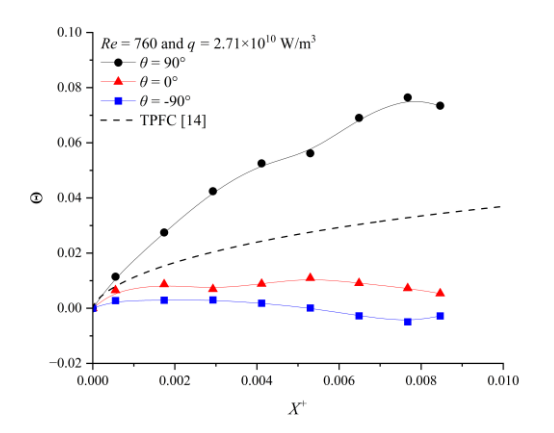


Fig. 6. Circumferential variation of axial Θ profiles (Re = 735 and $q = 2.71 \times 10^5 \text{ W/m}^3$).

3.4) Influence of the magnitude of the IHG (q)

Figures 7 shows the axial profiles of Θ_{avg} according to q at Re=1290. For the Θ_{avg} , the present results are lower than TPFC results. This reduction is attributed to the buoyancy induced D-shaped secondary flow, which enhances mixing and lowers the average wall temperature. As q increased, Θ_{avg} further decreased. This is due to the steepening of the temperature gradient between wall and bulk fluid which intensifies the D-shaped secondary flow.

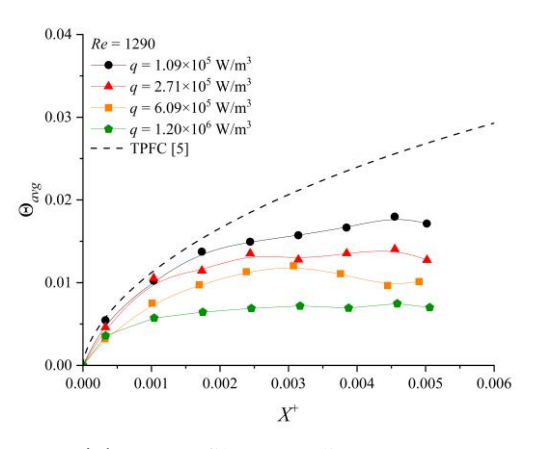


Fig. 7. Axial Θ_{avg} profiles according to q (Re = 1290).

Figures 8 shows the axial profiles of maximum values of Θ (Θ_{max}) which is the point at θ =90°. Θ_{max} is nearly two times higher than Θ_{avg} due to the thermal stagnation. Furthermore, in contrast to the Θ_{avg} which decreases with q, Θ_{max} is nearly not affected by q. This indicates that the thermal stagnant region remains largely unaffected by q.

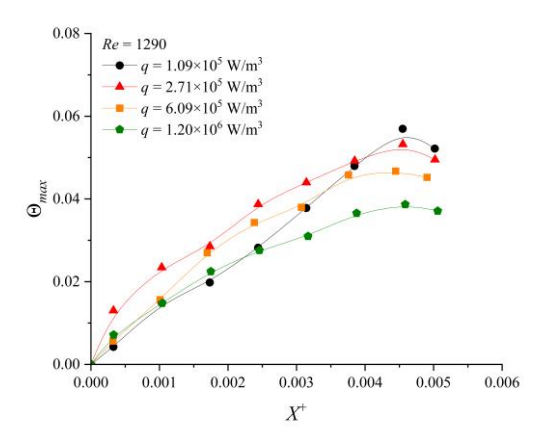


Fig. 8. Axial Θ_{max} profiles according to q (Re = 1290).

4. Conclusions

This study experimentally investigated the thermal-hydraulic behavior of horizontal laminar pipe flow with IHG under adiabatic wall boundary conditions. To simulate uniform volumetric heat generation, an alternating current was applied to an electrically conductive fluid.

Experimental results revealed that IHG induces significant thermal stratification due to buoyancy effects. A thermally stagnant region formed at the top of the pipe, while a D-shaped secondary flow developed beneath it. This secondary flow enhanced mixing in the lower region, resulting in reduced wall temperatures, whereas the stagnant region caused localized hot spots on the wall.

These findings indicate that under accident conditions, such as a pump trip, a low flow rate in the MSR can lead to the formation of local hot spots. These localized hot spots present potential risks to the system's integrity and safety.

Future research will aim to extend the range of investigation. Furthermore, rather than employing adiabatic wall conditions, experiments incorporating combined boundary conditions—such as wall heating or cooling—will be performed to more thoroughly examine the effects of IHG.

Nomenclature

c_p	Specific heat capacity [J/kg·K]
D	Pipe diameter [m]
I	Current [A]
k	Thermal conductivity [W/m·K]
L	Length of the test section [m]
ṁ	Mass flow rate [kg/s]
Q	Input power [W]
q	Volumetric heat generation rate [W/m³]
r	Radius of the pipe [m]
T	Temperature [K]
и	Velocity [m/s]

Uncertainty of variable i

 U_i

- V Voltage [V]
- x Streamwise distance [m]

Dimensionless numbers

- Grashof number, $g\beta\Delta TD^3/v^2$
- Gr^* Modified Grashof number, $g\beta qD^5/v^2k$
- Nu Nusselt number, hD/k
- *Pr* Prandtl number, v/α
- *Re* Reynolds number, uD/v
- X^+ Dimensionless axial distance, (x/D)/RePr
- Θ Dimensionless wall to bulk temperature
 - difference, $k(T_w-T_b)/qr_o^2$

Greek letters

- α Thermal diffusivity [m²/s]
- β Thermal expansion coefficient [1/K]
- θ Circumferential angle [°]
- v Kinetic viscosity [m²/s]
- ρ Density [kg/m³]

Acknowledgement

This study was also sponsored by the Ministry of Science and ICT (MSIT) and was supported by nuclear Research & Development program grant funded by the National Research Foundation (NRF) (No. RS-2025-02653218).

REFERENCES

- [1] M. Allibert, M. Aufiero, M. Brovchenko, S. Delpech, V. Ghetta, D. Heuer, A. Laureau, E. Merle-Lucotte, Molten salt fast reactors, in: Handbook of Generation IV Nuclear Reactors, 2016, pp. 157–188.
- [2] D. LeBlanc, Molten salt reactors: A new beginning for an old idea, Nuclear Engineering and Design, Vol. 240, 1644–1656, 2010.
- [3] C. Fiorina, A. Cammi, L. Luzzi, K. Mikityuk, H. Ninokata, M.E. Ricotti, Thermal-hydraulics of internally heated molten salts and application to the Molten Salt Fast Reactor, in: Journal of Physics: Conference Series, Vol. 501, IOP Publishing, pp. 012030, 2014.
- [4] H. Poppendiek, L. Palmer, Forced convection heat transfer in pipes with volume heat sources within the fluids, US Atomic Energy Commission, Technical Information Service, 1952.
- [5] E.M. Sparrow, R. Siegel, Laminar Tube Flow with Arbitrary Internal Heat Sources and Wall Heat Transfer, Nuclear Science and Engineering, Vol. 4, 239–254, 1958.
- [6] R. Siegel, E. Sparrow, Turbulent flow in a circular tube with arbitrary internal heat sources and wall heat transfer, Journal of Heat Transfer, Vol. 81, 280–287, 1959.
- [7] Y. Yang, Y. Zou, Evaluation of the thermo-hydraulic performance of molten salt in laminar flow with a uniform internal heating in a circular pipe, Applied Thermal Engineering, Vol. 268, 2025.
- [8] D.-H. Park, B.-J. Chung, Influence of internal heat generation on heat transfer in an MSR heat exchanger under laminar flow condition, Nuclear Engineering and Technology, Vol. 57, No. 103736, 2025.